This is a repository copy of *2D Material Microcavity Light Emitters:To Lase or Not to Lase?*.

Article:

Reeves, Lewis, Wang, Yue orcid.org/0000-0002-2482-005X and Krauss, Thomas F. orcid.org/0000-0003-4367-6601 (2018) 2D Material Microcavity Light Emitters:To Lase or Not to Lase? Advanced Optical Materials. ISSN: 2195-1071

2D Material Microcavity Light Emitters: To Lase or Not to Lase?

Lewis Reeves, Yue Wang, and Thomas F. Krauss*

Atomically thin layers of transition metal dichalcogenides (TMDs) are of great interest to the photonics community because of their unique optical properties. For example, in conjunction with microring or photonic crystal microresonators, they readily form microcavity light emitters. A number of configurations are now presented that apparently meet the conditions for lasing, yet there is considerable debate in the community as to whether lasing is actually achieved. By employing a very comprehensive set of assessment criteria, herein is shown that none of the TMD devices meet all the conditions for lasing, despite some very convincing data being presented. These findings are examined in the context of microcavity lasers based on III–V gain materials. Applications of TMD light emitters in the areas of quantum information and biosensing are also discussed to highlight areas where lasing action is not necessarily required.

1. Introduction

Interest in atomically thin materials was sparked by the "graphene revolution" initiated by the 2010 Nobel prize. In the wake of this achievement, a number of techniques for producing monolayers, such as mechanical exfoliation and chemical vapor deposition (CVD) growth, were developed. These techniques then opened the door for research into materials "beyond graphene" to explore what other functionalities may be realized, and transition metal dichalcogenides (TMDs) came to the fore. While graphene offers excellent mobility for electronic applications, the TMDs offer very high exciton binding energies, which is advantageous in photonics. TMDs have the general formula MX_2, where M is a transition metal and X is a chalcogen. Typical transition metals forming TMDs are Mo or W with the chalcogens being S, Se, or Te. It has been known for a while that thin layers of TMDs feature direct bandgaps in the visible and near-IR region of the optical spectrum[1] in contrast

L. Reeves, Dr. Y. Wang, Prof. T. F. Krauss
Department of Physics
University of York
Heslington, York YO10 5DD, UK
E-mail: thomas.krauss@york.ac.uk

The ORCID identification number(s) for the author(s) of this article can be found under https://doi.org/10.1002/adom.201800272.

to their indirect bandgaps observed in bulk, yet it took the graphene revolution to awaken this interest on a larger scale.

These direct bandgaps are found at the K and K′ valleys of the reciprocal lattice (**Figure 1**). The reason for the existence of two valleys at the K-point is that the inversion symmetry in the 2D Brillouin zone is broken by the alternate positioning of the transition metal and the chalcogen; hence the K point in each direction is different. The valleys are energy degenerate in momentum space; therefore, the interband transitions exhibit circular dichroism meaning that different transitions are coupled to right or left hand circularly polarized light. For an optically generated electron to change valley, it either has to flip its spin or it has to undergo an energetically unfavorable transition; hence the electron is both valley and spin-polarized. These valley-specific selection rules have given rise to a new area of research, "valleytronics,"[2] meaning that data could be stored or manipulated via different discrete values of the crystal momentum. At the K points, the spin degeneracy is lifted in both the conduction band (CB) and the valence band (VB), which is in contrast to, e.g., gallium arsenide quantum wells (GaAs QWs) where both CB and VB are spin degenerate. This spin-splitting effect gives rise to spin-allowed optically 'bright' transitions as well as spin-forbidden optically "dark" transitions.[3]

Light emission from TMDs is dominated by excitons and trions because of the strong Coulomb interactions inherent in the low dimensionality and the reduced dielectric screening compared to the bulk. These excitons (bound electron–hole pairs) have a very high binding energy (0.5–1 eV), which is one or two orders of magnitude higher than, e.g., that of GaAs QWs.[4] The high binding energy of the excitons leads to very short radiative decay rates on the order of 1 ps,[5,6] which is two orders of magnitude shorter than that of GaAs QWs. The transition metals and chalcogens can be combined almost arbitrarily within the MX_2 framework, and different combinations yield optical transitions of different energies, typically in the 1–2 eV range as illustrated in **Figure 2**.

2. Reports of TMD Microcavity Lasing Action

Based on these favorable properties, it is no surprise that researchers have sought to realize laser action using TMD gain materials. So far, all reported laser devices are optically pumped, but as we discuss later, electrical pumping is a real
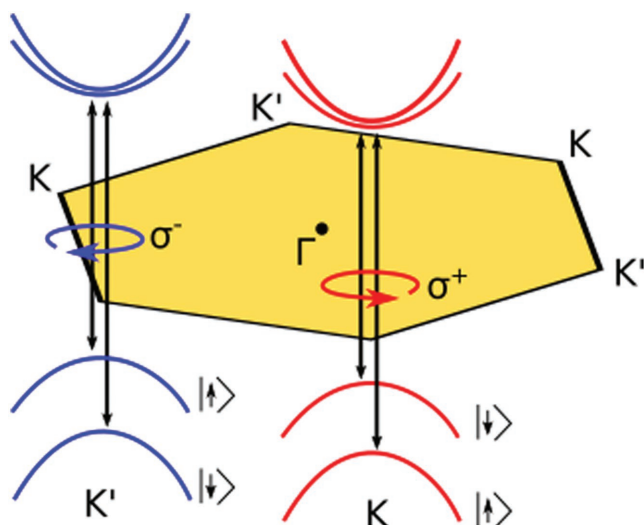
**ADVANCED
SCIENCE NEWS**

www.advancedsciencenews.com

**ADVANCED
OPTICAL
MATERIALS**

www.advopticalmat.de

Figure 1. Schematic bandstructure of monolayer TMDs showing the circular dichroism and the K and K' valleys.

possibility given the ability of forming sandwich structures with boron nitride as the insulator and graphene as the electrode.

2.1. WSe₂ Photonic Crystal Cavity Emitter

The first nanoscale laser was reported by Wu et al. in 2015.[10] The team transferred a monolayer of tungsten diselenide (WSe₂) onto an L3 photonic crystal (PhC) cavity fabricated in a gallium phosphide thin membrane (**Figure 3**a). Gallium phosphide was chosen as the substrate because its bandgap energy is higher than the WSe₂ emission energy. The L3 PhC cavity, which is a line defect cavity created by the removal of three adjacent holes, was tuned to be resonant around the PL peak at low temperature, i.e., 740 nm. The cavity exhibited a loaded Q-factor of 1300 at room temperature which increased to 2500 when the device was cooled to cryogenic temperatures.

A remarkable feature of this device was that the gain material was placed in the evanescent tail of the cavity, not at the center. Using finite-difference time-domain simulation (Figure 3a), however, the intensity of the lasing mode at the position of the monolayer was found to be 40% of the maximum, which showed that strong gain-cavity coupling can be achieved even via the evanescent tail.

The emission spectrum of the laser is shown in Figure 3d, obtained by pumping with a 632 nm continuous wave laser at 80 K. The device emits at 739.5 nm with a linewidth of 0.3 nm FWHM. The emission is polarized in the y-direction which is consistent with the cavity polarization. Figure 3b shows a plot of the output intensity as a function of incident pump power indicating lasing action at 130 K (b) and 80 K (c). The typical nonlinear "kink" in the L–L curve is clearly apparent. The β-factor, which is the fraction of spontaneous emission coupled into the lasing mode, was deduced by fitting the cavity laser rate equations. A β-factor of 0.19 was found to be the best fit as shown in Figure 3b. The threshold was found to be 27 nW corresponding to a pump density of ≈1 W cm⁻² and linewidth narrowing was observed around the lasing threshold (Figure 3e).

Lewis Reeves is a Ph.D. student in Photonics at the University of York, UK. He is interested in light emission from Silicon Photonic crystals. He is currently investigating TMDs as laser gain materials and ultrafast laser implantation (ULPI) of Er/Yb ions in glass also as gain materials as a part of the EPSRC SeaMatics project.
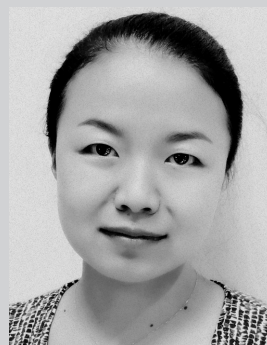
Yue Wang's doctoral research concerned the development of low threshold organic semiconductor lasers and sensors. In 2013, she joined the Photonics group at the University of York, to work on silicon-related nanostructures. Her current research interests focus on bringing together organic with inorganic, novel materials with engineered nanostructures, e.g., developing hybrid optoelectronics including optical material characterization (such as perovskite crystals and 2D materials) and subwavelength nanostructure design and fabrication, for light emission applications.

Thomas F. Krauss is Professor of Photonics at the University of York, UK. He has made pioneering contributions to the development of planar photonic crystal waveguides and cavities worldwide. His research interest is the light–matter interaction in such photonic nanostructures and he has led a number of EU and EPSRC projects on various aspects, such as slow light, optical interconnects and, more recently, novel photonic concepts for biosensing.

2.2. WS₂ Microdisk Cavity Emitter

Shortly after this first demonstration, Ye et al. presented a monolayer excitonic microcavity light emitter[11] based on a monolayer of tungsten disulfide (WS₂) placed onto a silicon nitride microdisk resonator. A schematic view of the device is shown in **Figure 4**a. A monolayer of WS₂ has a direct bandgap around 2 eV (Figure 2), corresponding to a photoluminescence peak at 610 nm. The WS₂ is sandwiched between the silicon
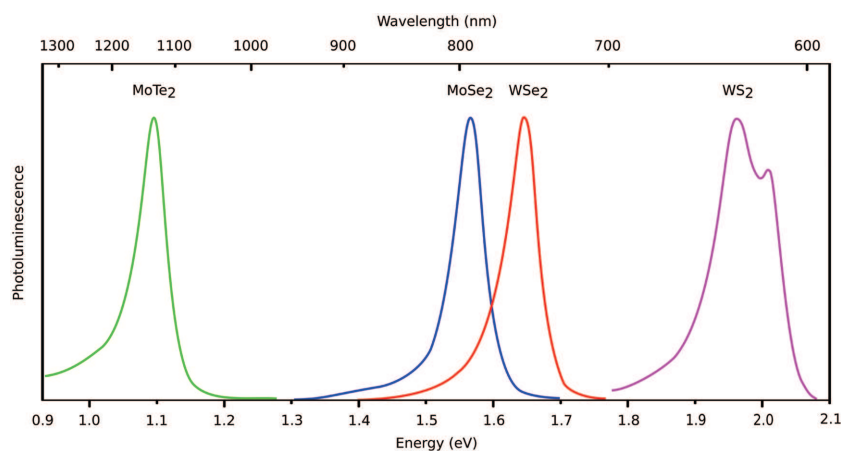
ADVANCED
SCIENCE NEWS
www.advancedsciencenews.com

ADVANCED
OPTICAL
MATERIALS
www.advopticalmat.de

Figure 2. Photoluminescence (PL) spectra of a variety of monolayer TMDs at room temperature. The PL intensities are each normalized to unity for ease of comparison. Data are shown for MoTe$_2$,[7] MoS$_2$,[8] WSe$_2$,[8] and WS$_2$.[9]

Q = 2604. The device was cooled to 10K and optically pumped with a 190 fs pulsed 473 nm laser and emission spectra collected via a 50 × objective. The emission characteristics as a function of pump power density are shown in Figure 4c. Above 22.4 MW cm^{-2}, the intensity of the peak at 612 nm increases sharply, suggesting lasing. A nonlinear "kink" in the L–L curve is shown in Figure 4b compared to the linear behavior of the background emission. A β-factor of 0.5 was determined from the fit shown in Figure 4b. The corresponding threshold analysis indicates a threshold value of around 5–8 MW cm^{-2}. The linewidth of the lasing mode was shown to narrow from 0.28 to 0.24 nm at threshold (Figure 4e).

nitride microdisk resonator and a thin layer of hydrogen silsesquioxane (HSQ) (Figure 4a), which serves to enhance the lasing mode overlap with the gain material, additionally encapsulating the WS$_2$ to prevent degradation by exposure to air. This encapsulation serves the additional purpose of increasing the optical confinement factor by ≈30% compared to the monolayer directly placed on the cavity. The microdisk structure was designed to have a diameter of 3.3 µm to give a strong TE polarized whispering gallery mode (WGM) resonance at 612 nm. The small diameter of the cavity increases the free spectral range hence there is only one mode available within the gain bandwidth. The Q-factor of the cavity is

2.3. The First Room Temperature Device: MoS$_2$ on a Microdisk

Also in 2015, Salehzadeh et al.[12] presented the first room temperature laser which was based on an MoS$_2$ laser operating at room temperature. Four-layer MoS$_2$ was placed on a freestanding SiO$_x$ microdisk cavity, illustrated in **Figure 5**a. The four-layer MoS$_2$ was treated with an O$_2$ plasma,[13] resulting in an increased PL intensity due to the decoupling of electronic states in individual layers. Using multilayer TMDs affords a higher optical confinement factor compared to a monolayer. The device was optically characterized at room temperature using a micro-PL setup with a 514 nm cw
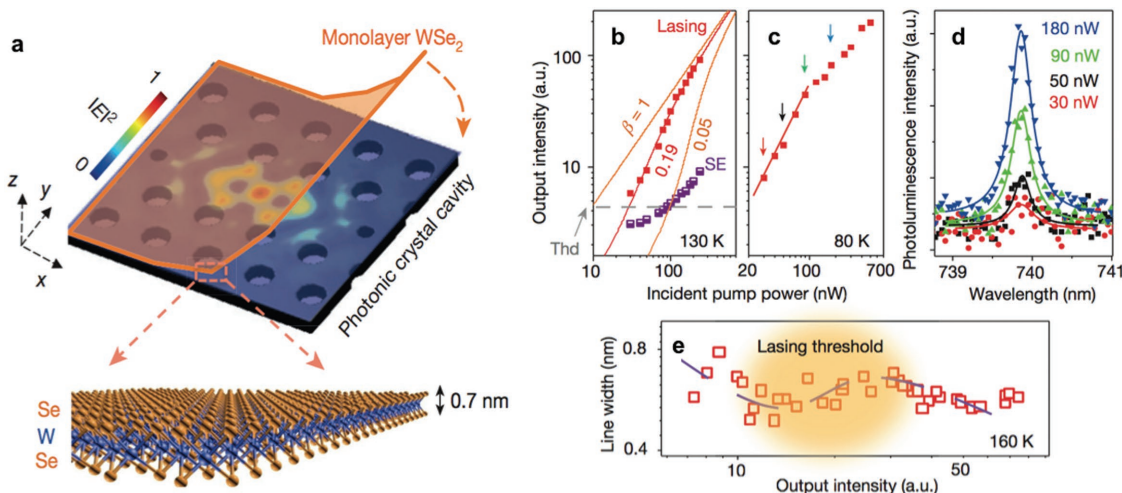

Figure 3. a) Cartoon depiction of the device architecture, where the electric-field profile (in-plane, x–y) of the fundamental cavity mode (pristine cavity before WSe$_2$ transfer) is embedded as the color plot. Inset: cartoon of the atomic structure of the monolayer. b) Light output intensity as a function of the optical pump power (L–L curve) at 130 K. Red filled squares correspond to the cavity emission. Violet half-filled squares correspond to the spontaneous emission (SE) off cavity resonance. Solid lines are the simulated curves using the laser rate equation with different β-factors. β = 0.19 is the best fit to the lasing data. Dark gray dashed line corresponds to the defined laser threshold, labeled by "Thd." c) L–L curve for the same lasing device at 80 K (red squares), where the solid line is a guide for the eye to the transition region. d) Photoluminescence spectra for increasing pump power. The solid lines are Lorentzian fits to the photoluminescence spectra. e) Cavity linewidth as a function of the detected output power at 160 K (open red squares). Dashed line is a guide to the eye to the nonlinear line width rebroadening area, which corresponds to the lasing threshold region. Reproduced with permission.[10] Copyright 2015, Springer Nature.
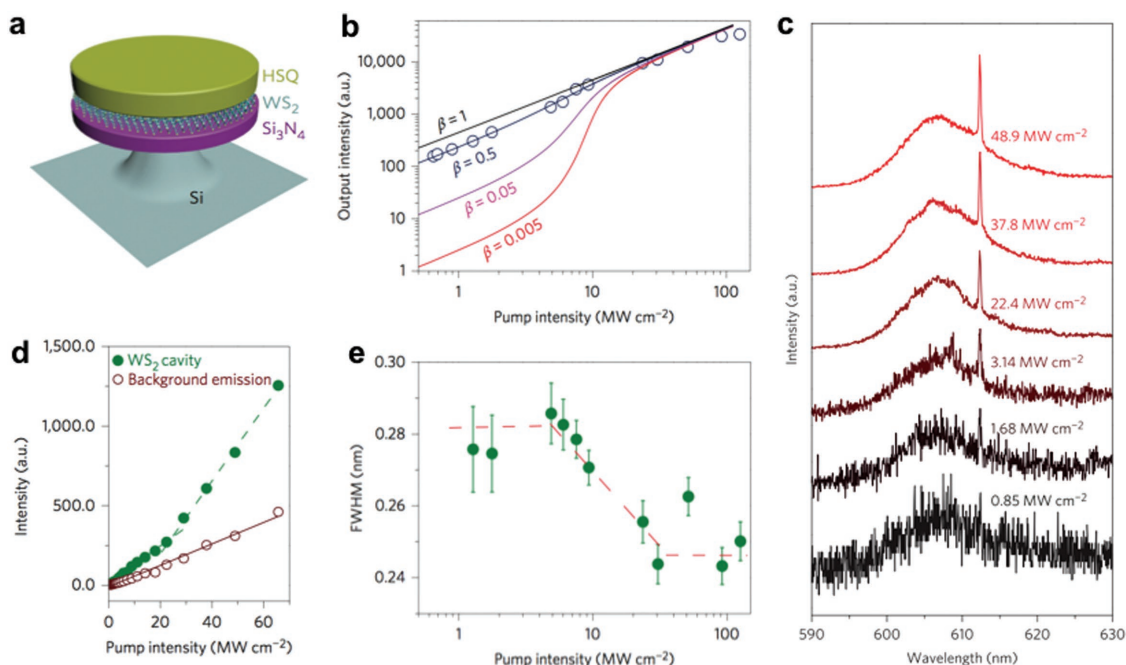
Figure 4. a) Schematic image of a monolayer WS$_2$ microdisk device highlighting the Si$_3$N$_4$/WS$_2$/HSQ sandwich structure. b) Experimental data and rate equation analytical fits. The best fit to the experimental data gives a threshold pump intensity of ≈5–8 MW cm^{-2} with a spontaneous emission factor, β, of 0.5. The fits to β of 0.005, 0.05, and 1 are also presented for comparison. c) Steady-state photoluminescence emission spectra with increasing pump intensity, normalized to pump intensity, illustrating the transition from spontaneous emission to stimulated emission and lasing. d) Monolayer WS$_2$ photoluminescence background and cavity emissions as a function of pump intensity. Dashed lines represent linear fits to the experimental data. The WS$_2$ photoluminescence background emission shows a linear dependence on the pump intensity, and the green dashed lines (cavity emission) show a kink indicating the onset of superlinear emission and lasing operation. e) FWHM versus input pump intensity. Linewidth narrowing of the lasing mode is observed as the excitation intensity exceeds the lasing threshold. The red dashed line is a guide to the eye. Reproduced with permission.[11] Copyright 2015, Springer Nature.

pump laser, using a silica microsphere to facilitate coupling (Figure 5a). At low pump power, below threshold, the characteristic WGM spectrum can be seen weakly superimposed on the PL background (Figure 5b). At higher pump powers, above threshold, The WGMs are enhanced by a factor of 20 whereas the background PL is only enhanced by a factor 2. Polarization dependent measurements were carried out showing that the observed modes were TE-polarized. Around the lasing threshold, a linewidth narrowing of the TE$^1_{52}$ mode from 0.36 ± 0.02 to 0.26 ± 0.02 nm was observed together with an abrupt change in slope of the L–L curve. The Q factor of the WGMs was measured to be in the range of 2600–3300. The

threshold power was estimated to be 20 μW (Figure 5c). The threshold pump power density was not reported.

2.4. Longer Wavelength TMD Emitters

The examples shown so far exhibited emission wavelengths in the near-IR below 1 μm, where III–V light emitters are readily available. Beyond the immediate scientific interest, it is difficult to envisage major applications for TMD light emitters in this wavelength range. This argument changes dramatically, however, once the wavelength exceeds 1.1 μm,

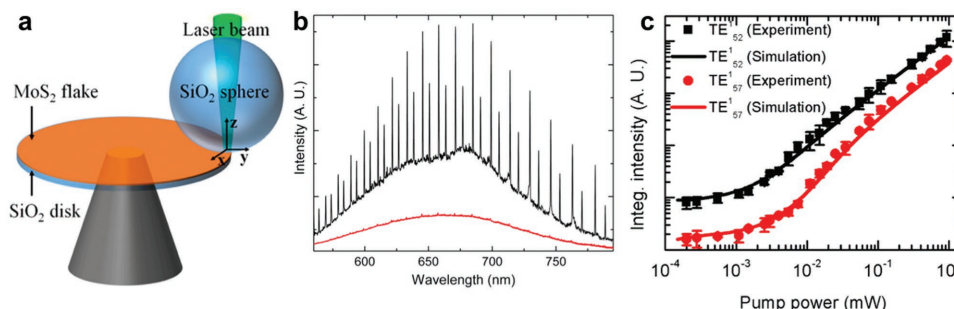**Figure 5.** a) Schematic configuration of the coupled microsphere/microdisk optical cavity with the incorporation of 2D MoS$_2$. b) RT-micro-PL spectra of the laser device with an excitation power of 3 μW (lower spectrum) and 30 μW (upper spectrum). c) L–L plot of the integrated intensity as a function of excitation power. Adapted with permission.[12] Copyright 2015, American Chemical Society.

ADVANCED
SCIENCE NEWS
www.advancedsciencenews.com

ADVANCED
OPTICAL
MATERIALS
www.advopticalmat.de

because the TMD then becomes compatible with silicon technology. Silicon technology affords the realization of some of the best microcavity resonators, and, more importantly, there is a real need for light emitters that can be directly integrated into silicon technology, in order to form optical interconnects. Optical interconnects offer a solution to the problem of high-speed data distribution on a chip, especially if the optical layer can be readily incorporated in the silicon process flow; TMD light emitters may provide this functionality.

Some TMDs exhibit optical gain at these longer near-IR wavelengths. For example, a monolayer of molybdenum ditelluride (MoTe₂) has a direct bandgap of 1.1 eV (1130 nm wavelength) and has already been used to make microcavity light emitters, as discussed next. Interestingly, a different type of 2D material, namely black phosphorous (BP), serendipitously bridges the gap between zero-bandgap graphene and the relatively large-bandgap TMDs, with bright 1300 nm wavelength photoluminescence having been demonstrated from three-layer BP.[14] There are no reports of devices yet, possibly because BP is relatively unstable and readily oxidizes when exposed to air.

Correspondingly, the first silicon-compatible TMD light emitter was presented by Li et al.[15] using a monolayer of MoTe₂ on a 1D silicon photonic crystal nanobeam cavity as illustrated in **Figure 6**b. Monolayer MoTe₂ has a bandgap around 1.72 eV but an excitonic photoluminescence emission peak exists at 1.1 eV, just below the bandgap of silicon. Silicon is only weakly absorbing at 1.1 eV, so transparent enough to support cavity modes of sufficiently high quality factor. The team measured their devices at room temperature pumping with 633 nm and obtained the spectra shown in Figure 6c. The first lasing mode

at 1052 nm has a significantly larger threshold of 0.426 mW compared to the 2nd mode at 1132 nm, because it experiences higher absorption from the silicon due to its shorter wavelength as well as less gain, being further away from the gain peak. The spontaneous emission exhibits a linear response to increasing pump power compared to the nonlinear behavior of the lasing modes shown in the L–L curves in Figure 6f. The linewidth of the 2nd mode at 1132 nm was measured to be 0.202 nm at 172 µW pumping power corresponding to a Q factor of 5603. This is the highest Q factor of any TMD laser demonstrated so far. The β-factor of 0.1 was deduced from fitting the laser rate equations. The threshold was determined from Figure 6f to be 0.097 mW corresponding to a pump density of 6.6 W cm⁻², although the authors used a very nonstandard method to obtain this pump density data. Applying standard methods, i.e., calculating the incident power density directly on the gain materials without taking absorption and coupling coefficients into account, based on the information given in the paper, we determined the pump threshold to be ≈2.1 kW cm⁻². We also note that Figure 6g plots a factor 2 reduction in the emission linewidth at threshold, although this factor 2 is not supported by the data shown in Figure 6d.

3. Criteria for Lasing

Having reviewed four examples of TMD light emitting devices, it is instructive to ask whether they actually meet the conditions for laser operation. To this end, we refer to the checklist of laser criteria published by Nature Photonics in 2017.[16] The list
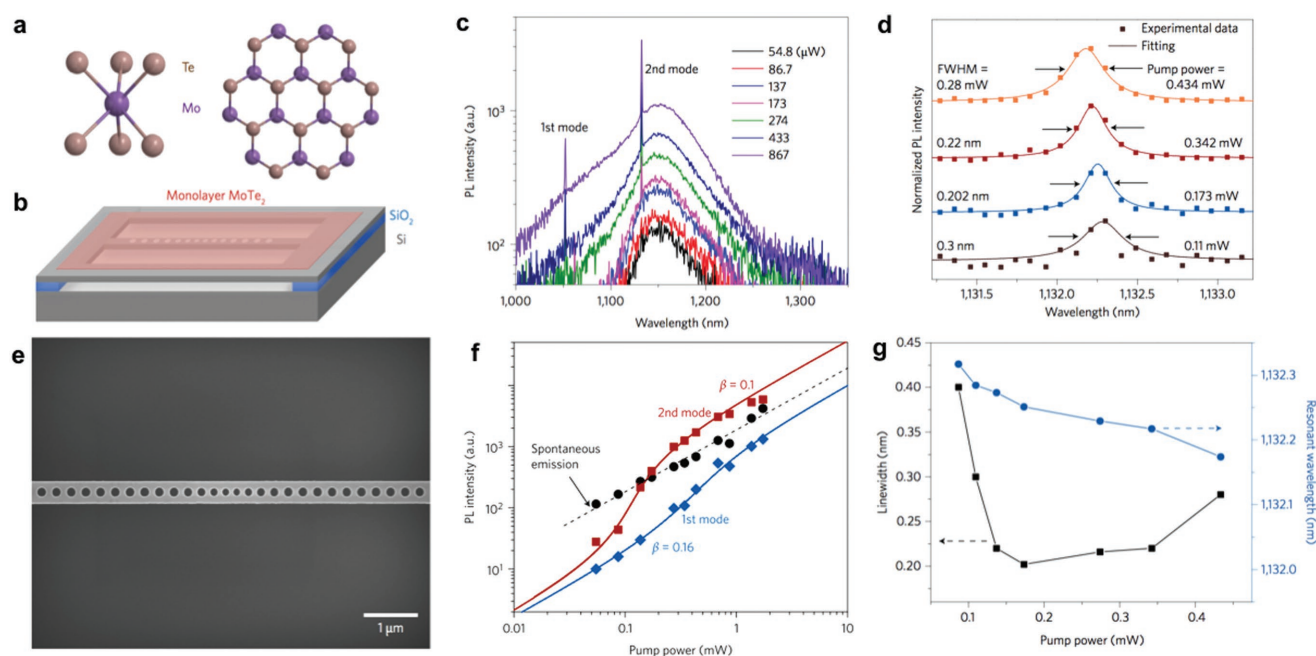

Figure 6. a) Crystal structure of MoTe2 (2H). b) Device schematic (silicon photonic crystal nanobeam laser structure suspended in air with a monolayer of MoTe₂ on top). c) PL spectra of the nanobeam light emitter with increasing pump power levels at room temperature. d) Fitting of the PL spectra for different pump levels. Solid squares represent the measured data points. The lines represent Lorentzian fits. e) SEM of an undercut silicon nanobeam cavity. f) Log–log plot of light in versus light out for the first two modes and for a background spontaneous emission. The solid squares represent data from experimental measurements, and the solid line is a rate-equation fitting. g) Linewidth (black) and resonant wavelength (blue), with arrows pointing to their respective axes, versus pump power. Reproduced with permission.[15] Copyright 2017, Springer Nature.

refers to a common set of data including threshold behavior, linewidth narrowing, polarization, and/or coherence together with recommendations of how best to represent the data to aid transparency and reproducibility. The list is partially based on a paper by Samuel et al.,[17] which was motivated by the same question ("How to recognize lasing") in organic semiconductor gain materials. Samuel et al. also highlighted threshold, linewidth narrowing, beamshape, and evidence of a cavity signature, together with coherence and polarization. We now assess the four examples in light of these criteria and we make the key point that coherence, which should be the ultimate criterion for lasing, is difficult to measure, hence the other conditions are often used as proxies. We also make the point that the second order correlation function, $g^{(2)}(t)$, underpins the other signatures.

It is clear from the table that the four examples, except for coherence, broadly meet the criteria outlined in refs. [16] and, [17] which at first sight supports their claims for lasing. These criteria are summarized in columns 2–6 of **Table 1**. Unfortunately, these conditions are not sufficient, especially for microcavity lasers, as we will discuss next.

3.1. Quantum Threshold Condition

Björk et al.[19] highlight that the conventional definition of a laser threshold, taken as the pump power required to make the net gain of the optical mode equal to the cavity losses, may not be sufficient for a microcavity laser. Instead, they suggest a more general definition of the lasing threshold as the point where stimulated emission overtakes spontaneous emission. For a microcavity mode in an active gain medium, this will occur when the mean photon number in the mode is unity. Correspondingly, $P_{th} \equiv 1$ where P_{th} is the mean photon number in the lasing mode. This condition is also known as the quantum threshold condition since it better describes the microscopic emission processes than the conventional definition does. To illustrate the quantum condition, let us consider the case of a microcavity laser. The best-case scenario occurs when the laser has a spontaneous emission factor of $\beta = 1$ and the cavity is loss-less, so the photon lifetime is only limited by the cavity lifetime. In this case, and starting from the definition of the cavity Q-factor as the ratio of the energy stored over the energy dissipated per photon cycle, we can calculate the photon lifetime in a cavity as follows

$$\tau = \frac{Q\, T_{cycle}}{2\pi} \tag{1}$$

As a representative example for the four TMD devices, we choose an operating wavelength of $\lambda = 0.9\ \mu m$ and a Q-factor of Q = 5000. From Equation (1) these values yield a cycle time of $T_{cycle} = 3$ fs and a cavity lifetime of $\tau = 2.4$ ps. This means that the cavity must emit a photon every 2.4 ps in order to meet the quantum threshold condition. Emitting a photon of 0.9 μm wavelength every 2.4 ps corresponds to an output power of ≈100 nW. Typical measurements only collect a fraction of the emitted photons, characterized by the collection efficiency, so one should measure an output power of order 10s of nW from a microcavity laser of Q = 5000. Unfortunately, none of the devices in Table 1 meet this criterion.

3.2. Linewidth Narrowing

While the standard laser conditions[16] already stipulate linewidth narrowing, a laser should actually meet the more stringent condition of linewidth narrowing by a factor 2. This factor 2 follows on from the quantum threshold. For example, Chow et al.[20] have investigated the intensity correlation characteristics of different types of light classified by the Hanbury–Brown–Twiss[21] experiment shown schematically in **Figure 7**a. Chow shows that for coherent laser emission, the equal-time second-order photon correlation $g^{(2)}(0)$ goes to unity.

In fact, the connection between the second order correlation function and coherence was first discussed by Mandel and Wolf in 1965.[22] As an example, Figure 7b shows the injection current dependency on the mean photon number. For the blue and black curves, as the injection current increases, the mean photon number in the cavity exceeds unity at around 10^{-5} A. At the same point of 10^{-5} A, $g^{(2)}(0) \Rightarrow 1$, signifying the onset of coherent emission (Figure 7c). This is further evidence for the quantum threshold, as at the point of quantum threshold, coherent emission occurs. Correspondingly, the linewidth narrows, as illustrated qualitatively in Figure 7a. As the photon emission becomes more regular, and by considering the Fourier transform in the frequency domain, we can see that the linewidth of the emission must narrow as the emission pattern changes from "bunched" to "random."

The Schawlow–Townes equation then provides a quantitative assessment of the linewidth reduction on threshold.[23] A good description of this effect is also found in chapter 11 of Siegman.[24] When a laser reaches threshold, it changes from an incoherent Gaussian noise source into a coherent sinusoidal oscillator. The Schawlow–Townes Equation (2) then stipulates that the linewidth must be modified by a factor of 2 (Equation (3)), as follows

Table 1. Comparison of the four TMD light emitters in light of the lasing conditions put forward.[16,17]

Device	Threshold	Linewidth narrowing	Beam	Polarization	Coherence	Quantum threshold	Linewidth narrowing by factor 2
WSe₂ PhCC	Yes	Yes	Yes[a]	Yes	Not shown	No	No
WS₂ microdisk	Yes	Yes	Not shown	Yes	Not shown	No	No
MoS₂ microdisk	Yes	Yes	Not shown	Yes	Not shown	No	No
MoTe₂ nanowire	Yes	Yes	Not shown	Not shown	Not shown	No	Not clear[b]

[a]Details of directional emission from the PhC cavity is presented in ref. [18]; [b]The authors claim linewidth narrowing by a factor 2, but this is not supported by the data shown.
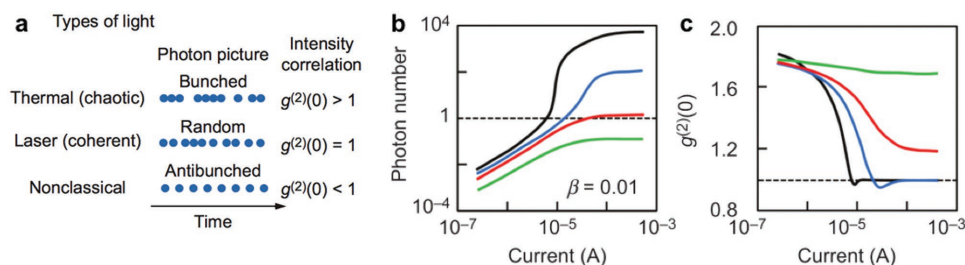
Figure 7. a) Different types of light classified by a Hanbury–Brown–Twiss measurement. Injection current dependences of b) photon number and c) equal-time second-order photon correlation for an emitter consisting of 50 quantum dots in a cavity with a spontaneous emission factor $\beta = 0.01$. The different curves correspond to photon loss rates $\gamma_c = 10^{10}$ s^{-1}, 5×10^{10} s^{-1}, 10^{11} s^{-1}, and 5×10^{11} s^{-1}. Reproduced with permission.[20] Copyright 2014, Springer Nature.

Above threshold:

$$\Delta\omega_{osc} = \frac{N_2}{N_2 - N_1} \times \frac{\pi\hbar\omega\Delta\omega_c^2}{P_{osc}} \qquad (2)$$

Below Threshold:

$$\Delta\omega_{osc} = 2 \times \frac{N_2}{N_2 - N_1} \times \frac{\pi\hbar\omega\Delta\omega_c^2}{P_{osc}} \qquad (3)$$

where N_1 is the photon occupancy of the lower state, N_2 the photon occupancy of the upper state, $\Delta\omega_c = \omega/Q_c$ the "cold cavity" linewidth and P_{osc} the free running output power of the laser.

These considerations make it clear that the linewidth should narrow by a factor 2 on threshold. We note that while all of the four devices report a linewidth reduction, none of them provide the data to demonstrate a reduction by the full factor 2 or preferably, a $g^{(2)}(0)$ measurement indicating coherent emission.

A further illustration of the relevance of the $g^{(2)}(0)$ measurement is provided by Kreinberg et al.,[25] who recently investigated emission from quantum-dot microcavities. They investigated three classes of devices, i.e., LEDs, cavity-enhanced LEDs, and microcavity lasers. While it was easy to distinguish between the LED and the laser, it was much more difficult to distinguish between cavity-enhanced LED and the laser, as both showed

the similar L–L plots coupled with linewidth narrowing, which could be mistaken for lasing. However, it was not until the equal-time intensity correlation $g^{(2)}(0)$ was examined when the difference between cavity-enhanced LED operation and lasing became apparent. Figure 8 illustrates that for the cavity-enhanced LED (b) $g^{(2)}(0)$ remains around 2 indicating thermal emission, whereas the laser (c) is the only device whereby $g^{(2)}(0)$ transitions to unity at the lasing threshold thereby indicating coherent emission.

3.3. Beta-Factor

The beta-factor is the fraction of spontaneous emission coupled to the lasing mode, and several papers use it to explain the very "soft" lasing threshold observed for their devices. As Kreinberg et al.[24] underline, however, the threshold behavior is not a strong indicator of lasing operation and it may be caused by a large fraction of spontaneous emission being present. As a reality-check, it is useful to consider the lambda-scale embedded active region photonic crystal (LEAP) laser described in detail in Section 5. This type of microcavity laser, which, as we show, displays all the relevant characteristics for lasing, shows a clear kink in the L–L curve and a beta-factor of 0.1 with a Q-factor of 3000. It is difficult to explain how other devices could obtain higher beta-factors given that they have similar or lower Q/V values.
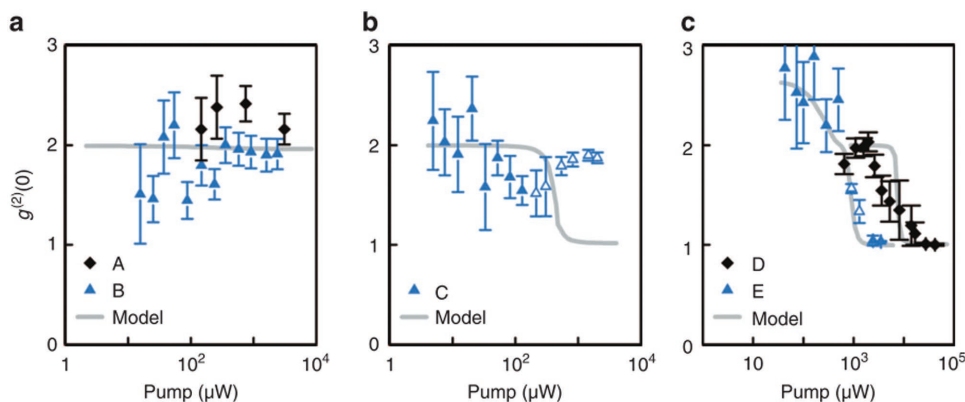

Figure 8. Equal-time intensity correlation versus pump power for QD-micropillar a) LED, b) cavity-enhanced LED, and c) laser. The gray curves represent theory. The data points are from experiment, where the solid symbols indicate $g^{(2)}(0)$ analysis by integration and the open symbols indicate fits considering the instrument impulse response of the setup. Reproduced with permission.[25] Copyright 2017, Springer Nature.

ADVANCED
SCIENCE NEWS
www.advancedsciencenews.com

ADVANCED
OPTICAL
MATERIALS
www.advopticalmat.de

4. Explanation of Apparent Laser Conditions

As we have now shown that none of the four examples meet the more stringent criteria for lasing of Table 1, we need to ask why the devices exhibit threshold behavior, polarization and beamshape? We believe that this question can be answered via condition 6 of the Nature Photonics list, which queries whether "alternative explanations, e.g., amplified spontaneous emission, directional scattering, modification of fluorescence spectrum by cavity, have been ruled out as being responsible for the emission characteristics?"[16]

Regarding polarization and beamshape, these may well be imprinted onto the beam by the cavity mode without requiring lasing, as the example of a photonic crystal cavity clearly demonstrates. As shown by Lo Savio[26] a photonic crystal cavity readily provides laser-like emission through resonant enhancement of the cavity mode. This emission is linearly polarized (otherwise, the resonant scattering method[27] would not be possible) and the cavity can provide a directed beam, especially if suitable beamshaping techniques such as "farfield optimization" are being employed.[28] Therefore, polarization and beamshape are not sufficient to explain laser operation.

Regarding the threshold condition and the observed linewidth reduction, the papers provide insufficient data, but we propose two possible explanations for this behavior, namely (1) that these effects may be caused by amplified spontaneous emission and/or (2) that the output of the laser may be pulsed.

(1) Amplified spontaneous emission (ASE) is defined as spontaneously emitted photons amplified by stimulated emission in a single pass through the gain medium. ASE can easily be mistaken for laser emission, especially in a high Q resonator, because resonator-scattered ASE and laser emission share many properties, including the characteristic nonlinear "kink" in the L–L curve, the linewidth narrowing, polarization and directionality of the output beam. In fact, laser emission from a high-gain medium always starts with ASE in presence of a resonator. The observations of the characteristic kink and linewidth narrowing are therefore not a sufficient condition[25] and as discussed above the second order

correlation function must be examined for evidence of coherence via the Hanbury Brown and Twiss experiment.[21]

(2) A different explanation is that the lasers may be self-pulsating, whereby the quantum threshold is met for a short time duration only. This scenario would explain the low output power while the device would still exhibit laser-like characteristics, such as the characteristic "kink;" the device may be operating as a passively mode-locked laser based on the well-known saturable absorption properties of TMDs.[29] To investigate the plausibility of this explanation, the emission of the laser could be measured using an ultrafast detector with picosecond time resolution, such as a streak camera; the time-dependent emission of the laser would then become evident. Since the output would be coherent if the quantum threshold condition was met for the duration of the pulse, second order photon correlation measurements, should also be successful. What about the linewidth narrowing at lasing threshold? We would expect the linewidth of a pulsed laser to be wider than that of a cw laser, as according to Fourier analysis, a short pulse exhibits a wider range of frequencies than a long pulse. Hence, such broadening would screen the factor 2 narrowing at the lasing threshold.

5. III–V Microcavity Lasers

To illustrate the fact that all the conditions of Table 1 can indeed be met, we now describe the example of a III–V based microcavity laser. We choose the LEAP laser developed at NTT, Japan, as an example.[30] Here, an InGaAlAs multiple quantum well active gain medium is embedded within an InP photonic crystal. Different regions of the photonic crystal are p- and n-doped to form a lateral p–i–n junction and enable current injection (**Figure 9**a). The laser emission is in the plane of the device and a waveguide is placed next to the active region to couple light out of the device. The cold cavity Q was determined to be 3000 with a β-factor of 0.1, however the Q-factor at threshold increased to 32 600. The output power in the waveguide as a function of driving current is shown in Figure 9b. A clear lasing threshold is seen at 7.8 µA, which is amongst the
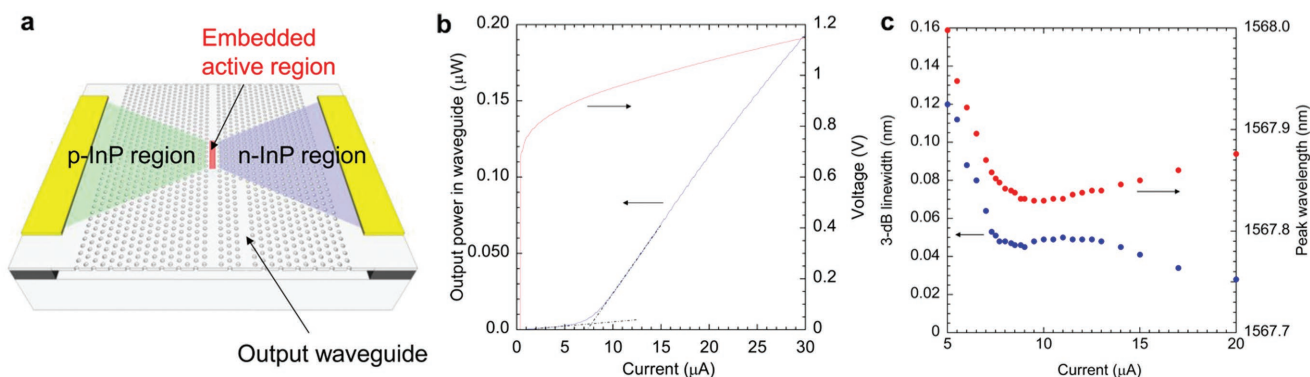

Figure 9. a) Schematic diagram of a fabricated electrically driven LEAP laser with a lateral current injection structure. b) Close-up near threshold region. The device exhibits a clear kink at a threshold of 7.8 µA. The output power coupled to an output line-defect waveguide was increased to 9.3 µW when the injection current was 300 µA. c) Injection current dependence on the 3 dB bandwidth of the peak and the peak wavelength. In the threshold region around 8 µA, the linewidth broadened with increasing output power. The 3 dB linewidth at threshold was 0.048 nm, corresponding to a Q-factor of 32 600. Reproduced with permission.[30] Copyright 2013, IEEE.

**ADVANCED
SCIENCE NEWS**
www.advancedsciencenews.com

**ADVANCED
OPTICAL
MATERIALS**
www.advopticalmat.de

lowest of any semiconductor laser ever reported. Next, the linewidth characteristics around the threshold were investigated (Figure 9c). A clear narrowing by more than a factor 2 is observed, reducing the linewidth from 0.12 to 0.05 nm, thereby clearly meeting the Schawlow–Townes condition. As this laser was designed for on-chip optical interconnects, it was also operated in direct electrical modulation and a maximum bandwidth of 16.2 GHz was demonstrated.

6. Applications of TMD Light Sources

The debate of whether 2D material microcavity light emitters are lasers or not should not distract from the fact that they are very versatile light sources, as 2D materials can be readily placed on almost any optically compatible substrate and electrical injection is a realistic prospect (see Section 7). Importantly, a number of reports have now also demonstrated that well-defined mono- and multilayer TMDs can be produced by CVD on a large scale,[31] opening the door toward upscaling and the potential for CMOS compatibility.

6.1. Integrated Optical Sensors

An area that could benefit from low-cost, scalable light sources integrated on silicon is refractive index sensing for biomedical or environmental applications. Such a sensor typically consists of an optically resonant or an interferometric transducer. If some target molecule binds to the surface of the sensor, the spectral position of the resonance or the interference pattern changes, which is picked up with a tunable source, a spectrometer or a detector array. The ultimate detection limit of such a sensor is determined by the noise of the photodetector and the signal to noise ratio against the source signal. Correspondingly, and given that the noise equivalent power of typical detectors is in the fW/$\sqrt{Hz}$ to low pW/$\sqrt{Hz}$ range, a high pW or low nW-level light source in a well-designed optical system would then be adequate for achieving a sufficient signal/noise ratio. The main difference compared to communications applications is that integration times can be much longer, i.e., while µW-levels of power are required for Gbit/s data rate applications,[32] sensing applications can easily afford second-level integration times and therefore require much lower optical powers to reach the required signal to noise ratios.

6.2. Single Photon Sources for Quantum Information

Single photon sources are an area of active research in the context of quantum information, where the quantum state of a single photon carries the information, in particular for quantum key distribution. Individual atoms, molecules, quantum dots, and color centers are all able to emit single photons. An ideal single photon source would have a 100% probability of emitting a single photon only while it would have a 0% probability of emitting multiple photons at the same time. These photons should be indistinguishable and be emitted at a fast rate.[33] TMD monolayers offer single photon emission by creating in the 2D sheet that act as confinement centers, similar to quantum dots. In order to create such nonuniformities, research has centered on nanoscale strain engineering, whereby monolayers have been placed on top of nanopillar arrays. The TMDs then conform to the surface topology of the nanopillars and the induced strain creates a confinement potential. Such strain-induced single photon emission has been observed in a range of monolayer TMDs such as WS_2,[34] WSe_2,[34,35] and $MoSe_2$[36] with second order photon correlation $g^{(2)}(0)$ measurements achieving near-zero correlation, indicating photon antibunching and the quantum nature of the emission. Moving to TMDs that emit at near-IR wavelengths where optical fibers exhibit their lowest losses and where they can be coupled directly to silicon photonic circuits[37] would make a large step toward realizing practical devices for quantum information.

7. Discussion and Conclusion

We have described a number of representative examples of microcavity light emitters based on TMD materials reported in the literature to date, all of which claim lasing action based on a careful analysis of the light input–output curve, demonstrating the characteristic "kink" in the curve that is traditionally seen as evidence for lasing. Starting with the Nature Photonics list,[16] we have conducted a more comprehensive analysis of lasing parameters and find that none of the devices meet these more comprehensive criteria, most notably that none of the devices evidence coherence. Since coherence from microcavity light emitters cannot be readily measured (e.g., via Young's slits), more indirect methods must be used that ultimately relate back to the second order correlation function $g^{(2)}(t)$. We also note that none of the devices achieve the quantum threshold condition that requires a minimum of one photon to be present in the cavity on average, or the linewidth that, according to the Schawlow–Townes condition, should reduce by a factor 2, which none of the devices have achieved. Finally, we verify our assessment framework by discussing a III–V based microcavity laser that indeed meets all of the criteria.

Going forward, we hypothesize that the characteristic "kink" in the output curve observed in all reports may be due to amplified spontaneous emission, or it may be due to some self-pulsating mechanism whereby the device emits laser radiation in short bursts. This hypothesis could be tested by conducting time-resolved measurements or by measuring the second order photon correlation $g^{(2)}(0)$ function $g^{(2)}(t)$ with sufficient time resolution.

Irrespective of the reason for failing the lasing criteria at this point, it is clear that TMD microcavity light emitters can be improved to achieve cw laser operation. We suggest the following routes:

a) Increase the gain volume. To increase the gain of the TMD layers, one could increase the number of layers and create a multilayer TMD heterostructure, alternating, e.g., with hexagonal boron nitride (h-BN) as the insulator to increase the available gain material. The same argument can be used to extend the length of the cavity; instead of a wavelength

scale L3-type or a nanobeam-type photonic crystal cavity, one can envisage making larger cavities that are able to draw on a larger gain volume, such as longer line defects or distributed coupled-cavity type configurations[38] that would still offer single mode operation within the gain spectral window.

b) Higher Q cavity. The quantum threshold condition is based on the photon lifetime in the cavity, so with a higher Q-factor, the photon lifetime could be extended.

c) Encapsulation. The TMD layer can be encapsulated with spin-coatable thin films such as PMMA or HSQ to prevent degradation from exposure to air. Encapsulation serves a dual purpose, e.g., by coating the cavity with a thin film of higher refractive index than air, the cavity mode will extend further from the cavity, thereby increasing the modal overlap with the TMD layer. This approach was already shown by Ye et al.[11] who reported an increase of the optical confinement factor by ≈30% compared to placing the monolayer directly on the cavity.

d) Electrical pumping. Electrically pumped lasers are a major step toward integration into on-chip devices, as shown by the LEAP laser where lasing was first demonstrated via optical pumping[32] before electrical pumping was realized.[30] 2D materials provide a viable route to electrically pumped operation. Graphene has high carrier mobility so can be used as the conductor, h-BN has a large bandgap and serves as the insulator, together with the TMD acting as the light emitting semiconductor.[39] Correspondingly, electrically pumped single-defect light emission from monolayer WSe_2[40] and a $MoTe_2$ light emitting diode[41] has now been demonstrated. Clearly, the next major goal is to demonstrate electrically pumped laser action in such sandwich structures. Intriguingly, if the saturable absorption properties of the TMD are responsible for the self-pulsation discussed above, then applying a suitable bias may allow to control the self-pulsating phenomenon as well.

Conflict of Interest

The authors declare no conflict of interest.

[1] J. A. Wilson, A. D. Yoffe, *Adv. Phys.* **1969**, *18*, 193.
[2] K. Behnia, *Nat. Nanotechnol.* **2012**, *7*, 488.
[3] M. Koperski, M. R. Molas, A. Arora, K. Nogajewski, A. O. Slobodeniuk, C. Faugeras, M. Potemski, *Nanophotonics* **2017**, *6*, 1289.
[4] G. Wang, A. Chernikov, M. M. Glazov, T. F. Heinz, X. Marie, T. Amand, B. Urbaszek, *Rev. Mod. Phys* **2018**, *90*, 21001.
[5] C. Robert, D. Lagarde, F. Cadiz, G. Wang, B. Lassagne, T. Amand, A. Balocchi, P. Renucci, S. Tongay, B. Urbaszek, X. Marie, *Phys. Rev. B* **2016**, *93*, 1.
[6] M. Palummo, M. Bernardi, J. C. Grossman, *Nano Lett.* **2015**, *15*, 2794.
[7] C. Ruppert, O. B. Aslan, T. F. Heinz, *Nano Lett.* **2014**, *14*, 6231.
[8] H. Zeng, G. Bin Liu, J. Dai, Y. Yan, B. Zhu, R. He, L. Xie, S. Xu, X. Chen, W. Yao, X. Cui, *Sci. Rep.* **2013**, *3*, 4908.
[9] M. Currie, A. T. Hanbicki, G. Kioseoglou, B. T. Jonker, *Appl. Phys. Lett.* **2015**, *20*, 201907.
[10] S. Wu, S. Buckley, J. R. Schaibley, L. Feng, J. Yan, D. G. Mandrus, F. Hatami, W. Yao, J. Vučković, A. Majumdar, X. Xu, *Nature* **2015**, *520*, 69.
[11] Y. Ye, Z. J. Wong, X. Lu, X. Ni, H. Zhu, X. Chen, Y. Wang, X. Zhang, *Nat. Photonics* **2015**, *9*, 733.
[12] O. Salehzadeh, M. Djavid, N. H. Tran, I. Shih, Z. Mi, *Nano Lett.* **2015**, *15*, 5302.
[13] R. Dhall, M. R. Neupane, D. Wickramaratne, M. Mecklenburg, Z. Li, C. Moore, R. K. Lake, S. Cronin, *Adv. Mater.* **2015**, *27*, 1573.
[14] J. Pei, X. Gai, J. Yang, X. Wang, Z. Yu, D. Y. Choi, B. Luther-Davies, Y. Lu, *Nat. Commun.* **2016**, *7*, 1.
[15] Y. Li, J. Zhang, D. Huang, H. Sun, F. Fan, J. Feng, Z. Wang, C. Z. Ning, *Nat. Nanotechnol.* **2017**, *12*, 987.
[16] *Nat. Photonics* **2017**, *11*, 139.
[17] I. D. W. Samuel, E. B. Namdas, G. A. Turnbull, *Nat. Photonics* **2009**, *3*, 546.
[18] S. Wu, S. Buckley, A. M. Jones, J. S. Ross, N. J. Ghimire, J. Yan, D. G. Mandrus, W. Yao, F. Hatami, J. Vučković, A. Majumdar, X. Xu, *2D Mater.* **2014**, *1*, 011001.
[19] G. Björk, A. Karlsson, Y. Yamamoto, *Phys. Rev. A* **1994**, *50*, 1675.
[20] W. W. Chow, F. Jahnke, C. Gies, *Light Sci. Appl.* **2014**, *3*, 1.
[21] R. Hanbury Brown, R. Q. Twiss, *Nature* **1956**, *178*, 1046.
[22] L. Mandel, E. Wolf, *Rev. Mod. Phys.* **1965**, *37*, 231.
[23] A. L. Schawlow, C. H. Townes, *Phys. Rev.* **1958**, *112*, 1940.
[24] A. E. Siegman, *Lasers*, University Science Books, Mill Valley, CA **1986**.
[25] S. Kreinberg, W. W. Chow, J. Wolters, C. Schneider, C. Gies, F. Jahnke, S. Höfling, M. Kamp, S. Reitzenstein, S. Hö, M. Kamp, S. Reitzenstein, *Light Sci. Appl.* **2017**, *6*, e17030.
[26] R. Lo Savio, S. L. Portalupi, D. Gerace, A. Shakoor, T. F. Krauss, L. O'Faolain, L. C. Andreani, M. Galli, *Appl. Phys. Lett.* **2011**, *98*, 1.
[27] M. Galli, S. L. Portalupi, M. Belotti, L. C. Andreani, L. O'Faolain, T. F. Krauss, *Appl. Phys. Lett.* **2009**, *94*, 2007.
[28] S. L. Portalupi, M. Galli, C. Reardon, T. Krauss, L. O'Faolain, L. C. Andreani, D. Gerace, *Opt. Express* **2010**, *18*, 16064.
[29] Z. Luo, D. Wu, B. Xu, H. Xu, Z. Cai, J. Peng, J. Weng, S. Xu, C. Zhu, F. Wang, Z. Sun, H. Zhang, *Nanoscale* **2016**, *8*, 1066.
[30] S. Matsuo, T. Sato, K. Takeda, A. Shinya, K. Nozaki, H. Taniyama, M. Notomi, K. Hasebe, T. Kakitsuka, *IEEE J. Sel. Top. Quantum Electron.* **2013**, *19*, 4900311.

[31] D. Zhu, H. Shu, F. Jiang, D. Lv, V. Asokan, O. Omar, J. Yuan, Z. Zhang, C. Jin, *npj 2D Mater. Appl.* **2016**, *1*, 8.

[32] C. Chen, K. Takeda, A. Shinya, K. Nozaki, T. Sato, Y. Kawaguchi, M. Notomi, S. Matsuo, *Opt. Express* **2011**, *19*, 17669.

[33] M. D. Eisaman, J. Fan, A. Migdall, S. V. Polyakov, *Rev. Sci. Instrum.* **2011**, *82*, 71101.

[34] C. Palacios-Berraquero, D. M. Kara, A. R. P. Montblanch, M. Barbone, P. Latawiec, D. Yoon, A. K. Ott, M. Loncar, A. C. Ferrari, M. Atatüre, *Nat. Commun.* **2017**, *8*, 1.

[35] A. Branny, S. Kumar, R. Proux, B. D. Gerardot, *Nat. Commun.* **2017**, *8*, 1.

[36] A. Branny, G. Wang, S. Kumar, C. Robert, B. Lassagne, X. Marie, B. D. Gerardot, B. Urbaszek, *Appl. Phys. Lett.* **2016**, *108*, 1.

[37] P. Lodahl, S. Mahmoodian, S. Stobbe, *Rev. Mod. Phys.* **2015**, *87*, 347.

[38] H. Altug, J. Vučković, *Opt. Express* **2005**, *13*, 8819.

[39] K. S. Novoselov, A. Mishchenko, A. Carvalho, A. H. Castro Neto, *Science* **2016**, *353*, aac9439.

[40] S. Schwarz, A. Kozikov, F. Withers, J. K. Maguire, A. P. Foster, S. Dufferwiel, L. Hague, M. N. Makhonin, L. R. Wilson, A. K. Geim, K. S. Novoselov, A. I. Tartakovskii, *2D Mater.* **2016**, *3*, 25038.

[41] Y.-Q. Bie, G. Grosso, M. Heuck, M. M. Furchi, Y. Cao, J. Zheng, D. Bunandar, E. Navarro-Moratalla, L. Zhou, D. K. Efetov, T. Taniguchi, K. Watanabe, J. Kong, D. Englund, P. Jarillo-Herrero, *Nat. Nanotechnol.* **2017**, *12*, 1124.

[42] A. Kumar, R. D. Schilling, N. Piro, S. Khorasani, M. Barbone, I. Goykhman, J. B. Khurgin, A. C. Ferrari, T. J. Kippenberg, C. Javerzac-Galy, A. Kumar, R. D. Schilling, N. Piro, S. Khorasani, M. Barbone, I. Goykhman, J. B. Khurgin, A. C. Ferrari, T. J. Kippenberg, *Nano Lett.* **2018**, *18*, 3138.

[43] H. Fang, J. Liu, H. Li, L. Zhou, L. Liu, J. Li, X. Wang, T. F. Krauss, Y. Wang, *Laser Photonics Rev.* **2018**, *12*, 1800015.

1800272 (11 of 11)